CRYSTAL GROWTH & DESIGN

pubs.acs.org/crystal

Article

Open Access

This article is licensed under CC-BY 4.0

Supramolecular Analysis of Six Novel Multicomponent Compounds of Substituted Salicylic Acids with Pyridine-Based Coformers

Published as part of the Crystal Growth & Design special issue "Multi-Component Pharmaceutical Solids".

Emmanuele Parisi,* Riccardo Montis,* and Luca Catalano*

Cite This: *Cryst. Growth Des.* 2025, 25, 7618−7627

Read Online

ACCESS | Metrics & More | Article Recommendations | Supporting Information

ABSTRACT: Crystallization of salicylic acid derivatives in the presence of either pyridine or 2-aminopyridine produced six novel crystal structures, covering most of the key components of the typical organic crystal form landscape. The six structures, which comprise salts, ionic cocrystals, solvates, and polymorphs, have been structurally compared and the influence of intermolecular interactions and molecular shape have been examined to identify any possible influence on the crystal packing and the energy frameworks of the different crystal forms.

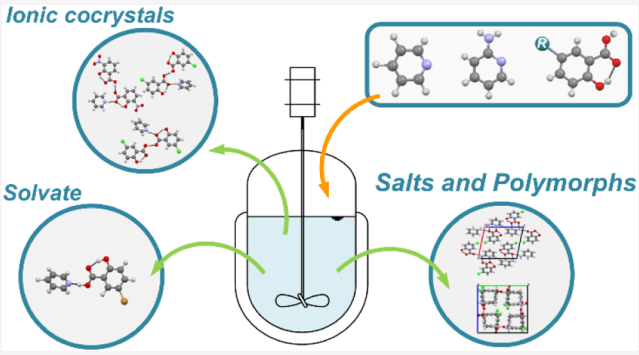

■ INTRODUCTION

Despite being often considered an old-fashioned concept, *Crystal Chemistry*, first introduced by Goldshmidt in 1926, posed the foundation of modern crystal engineering,[1] defining the rules that govern the intrinsic relationship between the chemical composition and the crystal structure of a given substance. In some respects, crystal chemistry and crystal engineering can indeed be regarded as two facets of the same medal. While the objective of crystal chemistry is to identify the relationships between the chemical composition and the crystal structures, crystal engineering uses this information to design new crystalline materials. According to the original idea behind *Crystal Chemistry*, a crystal can essentially be regarded as governed by the properties of its building blocks, such as the size, and the polarizability, and the knowledge of these parameters can be used to understand crystal structures. Although these observations were essentially obtained for inorganic compounds, the same principle can be applied to organic systems.[2] In this respect, Bragg in 1921, some years before the development of crystal chemistry, identified a close relationship between the unit cell parameters and the molecular size of naphthalene and anthracene.[3] Goldschmidt's work on crystal chemistry probably represents the earliest, if not the very first, example of a structural systematic study in crystallography. In the field of crystal engineering, such a systematic approach represents an important strategy to gain information on the factors determining or influencing crystal structures.[4−10] The main objective of crystal engineers is to design crystalline materials with specific properties.[11−15] This obviously involves a complete control of the crystallization process, including the ability of predicting the formation of specific molecular arrangements in the solid state.[16,17] However, this aspiration is constantly challenged by the observation that even small changes in the molecular structures might produce unpredictable self-assemblies in the solid state.[6,7,12,18,19] This might even be more challenging when multicomponent systems are taken into account. Organic multicomponent crystals have gained much interest for their potential application in the pharmaceutical and nutraceutical fields.[20−24] This has led to extensive research focused on exploring the supramolecular landscape determined by the formation of stable multicomponent adducts, with a specific focus on the structure and intermolecular interactions responsible for the association of the different components.[25−32]

Several studies have focused on the crystallization between electron-rich pyridine-N and benzoic acid derivatives.[5,33−39] In most of them, the results suggest that substituted groups can dramatically influence the crystal form landscape, promoting either competition or cooperativity among the set of intermolecular interactions available and driving the formation of specific supramolecular assemblies. Furthermore, they can also affect the relative acidity and basicity of the carboxylic and

Received: May 31, 2025
Revised: August 11, 2025
Accepted: August 12, 2025
Published: August 26, 2025

Downloaded via UNIV DEGLI STUDI DI URBINO on October 24, 2025 at 13:53:09 (UTC).
See https://pubs.acs.org/sharingguidelines for options on how to legitimately share published articles.

ACS Publications

© 2025 The Authors. Published by American Chemical Society

https://doi.org/10.1021/acs.cgd.5c00807
Cryst. Growth Des. 2025, 25, 7618−7627

pyridine functions, producing either salts or cocrystals. In the case of salicylic acid derivatives with pyridines, salt formation is often observed due to the presence of an intramolecular hydrogen bond assisted by resonance between the OH group in position 2 and carboxylic C═O, which stabilizes the carboxylate anion, increasing their acidity.[33]

Previous studies investigated the crystallization of a family of substituted salicylic acid derivatives in the presence of 4-aminopyridine.[33] Although the results showed significant structural variability, the system produced only salts due to the significant pK_a difference between the acids and the bases. In this study, we chose to investigate the crystallization of similar salicylic acid derivatives in the presence of a less basic coformer. We therefore targeted multicomponent systems based on pyridine derivatives and benzoic acid derivatives. Specifically, we analyzed the crystal structures of adducts of monosubstituted salicylic acid (**SA**) derivatives, such as 5-iodosalycilic acid (**5ISA**), 5-chlorosalycilic acid (**5ClSA**), 5-bromosalycilic acid (**5BrSA**), and 3-nitrosalycilic acid (**3NO$_2$SA**) with pyridine (**Py**) and 2-aminopyridine (**2APy**) (see Figure 1).

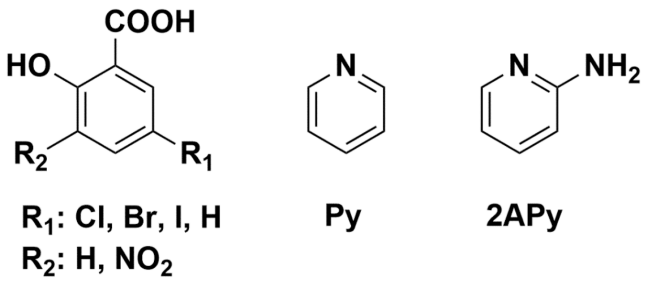

Figure 1. Molecular sketches of the salicylic acid derivatives and coformers.

The aim is to examine how the salicylic OH group and various substituents on the benzene ring influence the pyridine−carboxyl interaction. We therefore report the crystallization and the structural characterization of six novel adducts which involve solvates, salts, and ionic cocrystals (see Table 1) together with a complete analysis of their intermolecular interaction strength using CrystalExplorer software (v. 25.3a).[40]

■ EXPERIMENTAL SECTION

Sample Preparation. The **SA** derivatives (**5ISA**, **5ClSA**, **5BrSA**, and **3NO$_2$SA**) with a range of purity of 96−99%, were purchased from Acros Organics. **Py** and **2APy**, with a purity of 99%, were purchased from Sigma-Aldrich. All of the reagents were used without further manipulation.

Single-Crystal X-ray Data Collection and Structure Determination. Intensity data were recorded on a Nonius KappaCCD diffractometer situated at the window of a Bruker-Nonius FR591 rotating anode generator equipped with a molybdenum target (λ Mo−Kα = 0.71073 Å) and driven by COLLECT,[41] DirAx,[42] and DENZO softwares.[43] Structures were determined using the direct method procedure in SHELXT and refined by full-matrix least-squares on F^2 using SHELXL2016.[44] Data were corrected for absorption effects by means of comparison of equivalent reflections using the program SADABS.[45] Non-hydrogen atoms were refined anisotropically, while non-carboxyl or hydroxyl hydrogen atoms, although easily located in difference maps, were fixed in idealized positions with their displacement parameters riding on the values of their parent atoms. Carboxyl and hydroxyl hydrogens, also located in difference maps, were either included in the refinement with isotropic U_{iso} values or fixed in idealized positions, according to the general data quality for the structure. Full details of the crystal structure data for all new compounds are provided in Table 1.

Crystallization Procedure. Crystals suitable for single-crystal X-ray diffraction were obtained by slow evaporation from saturated solutions. The crystallization conditions are reported in Table 2.

Hydrogen Bond Statistics. The hydrogen bond statistics was performed with Mercury 2024.3.1 by comparing the hydrogen-bonding interactions of the six crystal structures with the CSD 5.46 database. The statistical comparison was performed using the following settings: the hydrogen atom had to be present, the acceptor and donor atom types were unrestricted, and the D−H···A angle was required to be ≥120°. The histograms obtained for each crystal structure are reported in the Supporting Information (Figures S1−S6).

Computational Methods. The intermolecular interaction energies were calculated with the CrystalExplorer 25.3a program package using the CE-B3LYP model and the 6-31G(d,p) basis set for molecules containing atoms from H to Kr and using the DGDZVP basis set for species containing heavier atoms.[46] The total interaction energies are portioned into Coulomb, dispersion, exchange, polarization, and repulsion.[47]

■ RESULTS AND DISCUSSION

Supramolecular Features and Interaction Energy Landscape. A summary of the crystal data of the six novel compounds is given in Table 1. All of the structures predominantly crystallize with $Z' = 1$, with the only exception being phase **4**, which crystallizes with two independent ion pairs (**4APy$^+$5ISA$^-$**) in the asymmetric unit. Crystal structures **2** and **6** are both ionic cocrystals with an asymmetric unit comprising a **Py$^+$SA$^-$** ion pair interacting with a neutral **SA** moiety. Structures **1**, **3**, and **4** represent organic salts formed by proton transfer from the **SA** derivative to the **2APy** base. In particular, structures **3** and **4** are polymorphic. As expected for ionic compounds, all of these structures feature strong ionic interactions between the **Py$^+$** and **SA$^-$** ions. The only structure that does not show ionic interactions is **5**, which crystallizes as a solvate, with an asymmetric unit consisting of neutral **5BrSA** and **Py** in a 1:1 stoichiometric ratio.

According to the ΔpK_a rule, when the difference in the pK_a values of the acid and the base is greater than 3, proton transfer from the salicylic acid derivative to **Py**/**2APy** is expected. Table S1 shows the reported pK_a values for all of the coformers. On the basis of these, salt formation was observed for ΔpK_a greater than 4, while solvates or ionic cocrystals formed when the values were in the range 2.5−3.2.[48,49] These results are consistent with previous evidence, which has shown that when $0 < \Delta pK_a < 4$, the crystallization is less predictable and can lead to the formation of salts, cocrystals, or ionic cocrystals, while for ΔpK_a values greater than 4, the product is typically a salt.[50,51]

In the case of the neutral structure **5**, the primary intermolecular interaction consists of a COOH···N hydrogen bond between the carboxylic function and the aromatic nitrogen, leading to an *anti*-configuration. On the contrary, in the case of the ionic structures, the electrostatic component supports a hydrogen bond similar in topology but significantly stronger, leading to a *syn*-configuration (Figure 2).

As shown in Figure 3, when **Py$^+$** interacts in the *syn*-configuration, the carboxylate group is always involved in a hydrogen-bonding interaction with the neutral **SA** derivative (**2** and **6**) along the *b* direction in **2** and along the *b* + *c* direction in **6**. Differently, in solvate **5**, where the **Py** interacts in the *anti*-configuration, the carboxylic oxygen interacts through a hydrogen-bonding interaction with another **Py** of the underlying layer. The carboxylic oxygens of the **SA** derivative molecules are always almost coplanar with the aromatic ring due to the

https://doi.org/10.1021/acs.cgd.5c00807
Cryst. Growth Des. 2025, 25, 7618−7627

Table 1. Crystallographic Data for the Six Adducts

	1	2	3	4	5	6
	5ISA-2APy	5ClSA-Py	5ClSA-2APy (I)	5ClSA-2APy (II)	5BrSA-Py	$3NO_2$SA-Py
	salt	ionic cocrystal	salt	salt	solvate	ionic cocrystal
chemical formula	$C_7H_4IO_3{\cdot}C_5H_7N_2$	$C_7H_5ClO_3{\cdot}C_7H_4ClO_3{\cdot}C_5H_6N$	$C_7H_4ClO_3{\cdot}C_5H_7N_2$	$C_5H_7N_2{\cdot}C_7H_4ClO_3$	$C_7H_4BrO_3{\cdot}C_5H_6N$	$C_7H_5NO_5{\cdot}C_7H_4NO_5{\cdot}C_5H_6N$
M_r	358.13	424.22	266.68	266.68	296.12	445.34
crystal system, space group	orthorhombic *Fdd2*	monoclinic $P2_1/n$	monoclinic $P2_1$	monoclinic $P2_1/c$	monoclinic $P2_1/n$	triclinic, *P-1*
a	25.5337 (6)	7.3275 (2)	10.0078 (4)	12.4607 (4)	3.9157 (4)	7.6293 (6)
b	28.3056 (7)	17.7071 (5)	5.1226 (2)	14.3841 (4)	21.599 (2)	11.5595 (10)
c	7.3948 (2)	14.3226 (5)	12.0370 (4)	14.3774 (3)	13.5839 (14)	11.8488 (8)
(Å)						
α	90	90	90	90	90	63.098 (4)
β	90	102.073 (2)	101.645 (2)	108.941 (1)	91.623 (6)	89.366 (5)
γ	90	90	90	90	90	84.813 (4)
(°)						
V (Å^3)	5344.6 (2)	1817.24 (10)	604.39 (4)	2437.41 (12)	1148.4 (2)	927.53 (13)
Z	16	4	2	8	4	2
μ (mm^{-1})	2.40	0.40	0.32	0.32	3.57	0.13
crystal size (mm)	0.4 × 0.2 × 0.1	0.12 × 0.1 × 0.08	0.8 × 0.2 × 0.1	0.15 × 0.14 × 0.04	0.5 × 0.08 × 0.08	0.12 × 0.06 × 0.04
diffractometer	Bruker-Nonius Roper CCD camera on κ-goniostat	Bruker-Nonius Roper CCD camera on κ-goniostat	Bruker-Nonius Roper CCD camera on κ-goniostat	Bruker-Nonius Roper CCD camera on κ-goniostat	Bruker-Nonius Roper CCD camera on κ-goniostat	Bruker-Nonius Roper CCD camera on κ-goniostat
absorption correction	multi-scan SADABS 2007/2 (Sheldrick, 2007)	multi-scan SADABS 2007/2 (Sheldrick, 2007)	multi-scan SADABS 2007/2 (Sheldrick, 2007)	multi-scan SADABS 2007/2 (Sheldrick, 2007)	multi-scan SADABS 2007/2 (Sheldrick, 2007)	multi-scan SADABS 2007/2 (Sheldrick, 2007)
N° of meas., ind. and obs. [$I > 2\sigma(I)$] refl.	10559, 2995, 2809	25129, 4175, 2785	9101, 2709, 2508	28830, 5583, 4130	12380, 2596, 1944	18845, 4270, 2082
R_{int}	0.031	0.105	0.037	0.061	0.086	0.126
$R[F^2 > 2\sigma(F^2)]$, $wR(F^2)$, S	0.025, 0.056, 1.09	0.060, 0.153, 1.04	0.034, 0.083, 1.06	0.067, 0.134, 1.11	0.082, 0.202, 1.14	0.078, 0.209, 1.00
N° of refl.	2995	4175	2709	5583	2596	4270
N° of par.	164	265	164	413	160	290
$\Delta\rho_{max}$, $\Delta\rho_{min}$ (e Å^{-3})	0.25, −0.60	0.35, −0.45	0.19, −0.23	0.29, −0.34	1.90, −0.94	0.38, − 0.51
abs. struc. par.	−0.007 (12)	7.3275 (2), 17.7071 (5), 14.3226 (5)	−0.03 (3)	−	−	−

https://doi.org/10.1021/acs.cgd.5c00807
Cryst. Growth Des. 2025, 25, 7618−7627

Table 2. Summary of the Crystallization Conditions for 1−6[a]

	component 1	component 2	solvent	CCDC numbers
1[a]	5ISA	2APy	methanol	2429637
2	5ClSA	Py	pyridine	2429654
3	5ClSA	2APy	methanol/water 1:1	2429655
4	5ClSA	2APy	pyridine	2429656
5	5BrSA	Py	pyridine	2429657
6	$3NO_2SA$	Py	pyridine	2429658

[a]Crystallization from pyridine produced the same unit cell.

formation of an intramolecular interaction with the hydroxyl group in ortho with torsion angle (τ_1) values from −4.7 to 6.2° (Table 3), in accordance with previous studies.[33]

The ionic character of the **SA**$^-$ derivatives is confirmed by experimental distances between C1 and the two oxygen atoms that fall in the range between 1.22 and 1.30 Å for carboxylic acids. Differently, for the solvate **5**, there is an inversion of the bond lengths because in this crystal structure, the carboxylic oxygen O1 is not anionic and retains the hydrogen atom. The distance between N−H$^+$···$^-$O is comparable for all of the crystal structures (see Table 4).

By looking at the hydrogen-bonding interaction in the crystal structures containing **Py**$^+$, as shown in Figure 4, the shorter distance between the donor atom and the acceptor atom can be related to the formation of ring motifs $R_4^4(14)$, $R_2^4(10)$, and $R_3^3(11)$. For compound **5**, the shortest distance can be accounted to the formation of the smallest ring among them.

In the crystal packing of **5** (Figure 5), the **Py** and **SA** moieties are arranged in layers, adopting a herringbone motif (with an angle between the two of 53.3(3)°), with an interlayer distance of 3.916(3) Å.

The crystal packings of the two ionic cocrystals **2** and **6** differ for both the orientation of the molecules and the supramolecular interaction patterns, as shown in Figure 6. In addition to the formation of the different supramolecular features described above, the presence of chlorine in **2** contributes to the formation of halogen interaction patterns that are absent in **6**. These interactions break the planar arrangement of the molecules in layers observed for **6** (Figure 6c,6d) by producing herringbone motifs through the formation of dimeric halogen interactions (Figure 6b). In both of the ionic crystal structures, the hydroxyl group of the neutral **SA** derivative is involved in hydrogen-bonding interactions with the carboxylate of **SA**$^-$ with distances of 2.54 Å (Table 2). In the crystal structure **6**, the nitro group is also involved in the C−H···O interaction with the aromatic rings by assisting the formation of planar layers (2.550(4) and 2.510(5) Å).

On the other hand, the COO-NHCNH$_2$ $R_2^2(8)$ supramolecular synthon (Figure 7) represents the robust feature in the crystal structures of **2APy**$^+$ and the **SA**$^-$ derivatives. The adducts **1**, **3**, and **4** differ only for iodine/chlorine in position 5 of **SA**. The amino group of **2APy**$^+$ is coplanar with the aromatic ring and is always involved in strong hydrogen-bonding interactions with carboxylate. Indeed, the distance between the donor N−H and acceptor oxygen is short (Table 2).

The packing of the molecules in **1** is very similar to that in structure **5**, in which **SA**$^-$ and **Py**$^+$ are piled up along the *b* axis in the ABAB theme (Figure 8a). Dimers of **SA**$^-$ and **Py**$^+$ are arranged face-to-edge, and they are held by a weak hydrogen-bonding interaction between the iodine and hydroxyl groups of **SA**$^-$ (3.224(3) Å, Figure 8b).

The last two crystal structures **3** and **4** are polymorphs of the **5ClSA** derivative. The crystal packing of **3** (Figure 9a) can be described similarly to **1**, but in this case, the molecules are stacked along the *b* axis by forming columns of **SA**$^-$ and columns of **Py**$^+$. The different columns are thus held not only by the supramolecular synthons described above but also around the 2_1-screw axis, where the chlorine atoms interact with each other through the formation of halogen bonds with a distance of 3.527(1) Å (Figure 10a). Differently, in the crystal packing of the polymorphic form **4**, the molecules are arranged in an orthogonal column (Figure 9b) composed by the **SA**$^-$-**Py**$^+$ pair.

In this case, chlorine is not involved in any halogen-bonding interaction but it interacts in a weak C−H···Cl interaction in a bifurcated way with C−H of the **Py**$^+$ aromatic ring (2.898(3) and 2.866(2) Å), as shown in Figure 10b.

Therefore, the interaction energy landscape of the analyzed compounds is dominated by four interactions: **SA**$^-$-**Py**$^+$, **SA**-**Py**$^+$, **SA**-**SA**$^-$, and **SA**-**Py**$^+$. The total interaction energies are reported in Figure 11 and Table 5. Due to the ionic character of the six adducts, the **SA**$^-$-**Py**$^+$ interaction is always present with total energy values between −454.6 and −363.7 kJ/mol, and the interaction energies are affected by the different crystal packing motifs in each crystal structure. This interaction is about four times greater than that between **SA**-**SA**$^-$ and about six times greater than that between **SA**-**Py**$^+$. As shown in Figure 11a, the adducts with **Py**$^+$ (**2** and **6**) show the lower value to the total energy of the electrostatic contribution, which can be related to two different reasons: in **2**, **Py**$^+$ and the **SA**$^-$ are not coplanar, as shown in Figure 2, promoting the formation of strong ring motifs; on the other hand, in the ionic cocrystal **6**, the presence of the nitro group has an electron-withdrawing effect on the negative charge of **SA**$^-$, making it less available to the electrostatic interaction. Differently, for the other compounds, the formation of strong **SA**$^-$···**2Apy**$^+$/**Py**$^+$ hydrogen bonds, as shown in Figure 7, makes the electrostatic interaction between **SA**$^-$ and **Py**$^+$ more efficient and stronger.

In addition to the **SA**$^-$-**Py**$^+$ interaction, ionic cocrystals **2** and **6** show a slight contribution of a charge-assisted hydrogen-bonding interaction between neutral **SA** and the two ionic

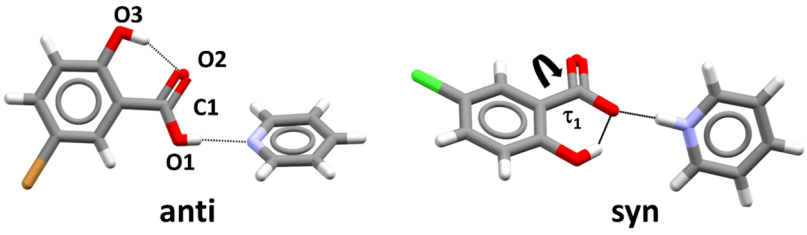

Figure 2. Supramolecular descriptors for the **SA**/**SA**$^-$ derivatives (**5** left and **2** right) and **Py**/**Py**$^+$ as the representative. *Anti*- and *syn*-configurations were used for **Py**/**Py**$^+$. τ_1 represents the torsion angle of the 2-hydroxycarboxylate group in the **SA**/**SA**$^-$ derivatives.

https://doi.org/10.1021/acs.cgd.5c00807
Cryst. Growth Des. 2025, 25, 7618−7627

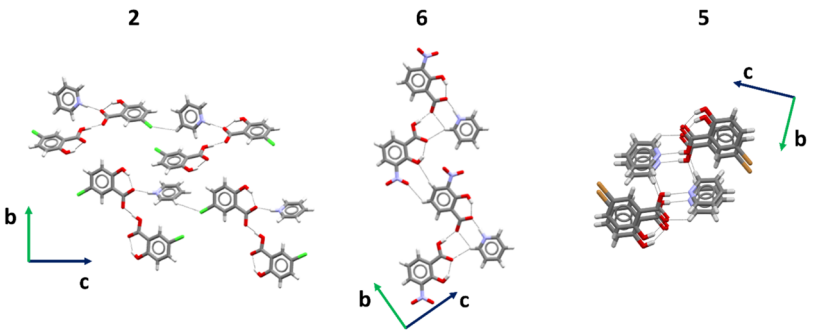

Figure 3. Hydrogen-bonding interactions of **Py**/**Py**$^+$ with **SA**/**SA**$^-$ derivatives.

Table 3. Supramolecular Descriptors As Shown in Figure 2

	C1−O1 (Å)	C1−O2 (Å)	O3···O2 (Å)	O3−H···O2 (Å)	τ_1(°)	Py/Py$^+$ config.
1	1.246(5)	1.268(5)	2.515(4)	1.771(4)	−4.6(6)	
2	1.259(3)	1.272(4)	2.603(3)	1.780(4)	−1.6(4)	syn
3	1.252(3)	1.284(3)	2.528(2)	1.784(3)	−1.4(3)	
4	1.244(3)	1.284(4)	2.546(3)	1.800(5)	6.2(4)	
5	1.293(8)	1.236(9)	2.601(7)	1.796(3)	−4.7(4)	anti
6	1.252(5)	1.273(4)	2.604(3)	1.721(4)	2.1(5)	syn

Table 4. Hydrogen Bond Donor−Acceptor Distances and Angles[a]

		distance D−A (Å)	distance mean (Å)	angle D−H (°)	angle mean (°)
NH$^+$···$^-$O	**1**	2.70	2.76	175.96	173.32
	2	2.63	2.74	165.94	173.17
	3	2.69	2.76	173.54	173.32
	4	2.67	2.76	174.72	173.32
	6	2.68	2.74	172.02	173.17
NH···O	**1**	2.86	2.88	177.93	173.40
	3	2.80	2.88	171.53	173.40
	4	2.82	2.88	159.51	173.40
OH···$^-$O	**2**	2.54	2.60	176.98	172.46
	6	2.54	2.60	174.25	172.46

[a]The mean values are calculated among the crystal structure hits found.

forms. The difference in the total energy value of the **SA**-**Py**$^+$ interaction between **2** and **6** is directly related to the hydrogen bond strength of the interaction. In **6**, the N−H$^+$···O hydrogen-bonding distance (1.617(3) Å) is much shorter than that in **2** (1.747(3) Å), resulting in roughly twice the magnitude of the total energy (−64.3 kJ/mol in **6** vs −32.7 kJ/mol in **2**). By looking at the crystal packing of **6** (Figure 6d), the higher contribution of the electrostatic interaction could be related to the formation of planar ribbons, which bring closer the molecules in the plane.

For structure **2**, the total energy of the **SA**-**Py**$^+$ and **SA**-**SA**$^-$ interactions arises from a balance, in which strong repulsive forces are countered by enhanced electronic and polarization components. As regards the charge-assisted hydrogen-bonding **SA**-**SA**$^-$ interaction, also in this case, the total energy is strongly influenced by the distances of OH-O$^-$ (−126.9 kJ/mol in **2** and −100.0 kJ/mol in **6**) with a shorter hydrogen-bonding distance in the ionic cocrystal **2** (1.536(3) Å) than that found in compound **6** (1.703(3) Å).

■ CONCLUSIONS

This study systematically explored the supramolecular and structural chemistry of six novel crystal forms derived from salicylic acid derivatives and pyridine-based coformers **Py**/**2APy**. The isolation of different solid forms within the crystal landscape, such as salts, ionic cocrystals, and solvates (or cocrystals), reflects the importance of substituent groups in determining the relative acidity and basicity of the chemical species involved in the formation of these multicomponent solid forms. In previously reported salts of salicylic acid and 4-

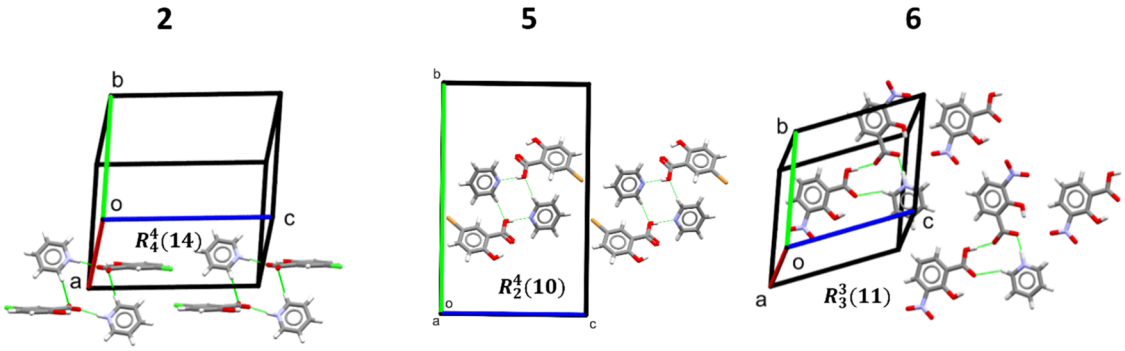

Figure 4. Ring motifs of compounds **2**, **5**, and **6**.

https://doi.org/10.1021/acs.cgd.5c00807
Cryst. Growth Des. 2025, 25, 7618−7627

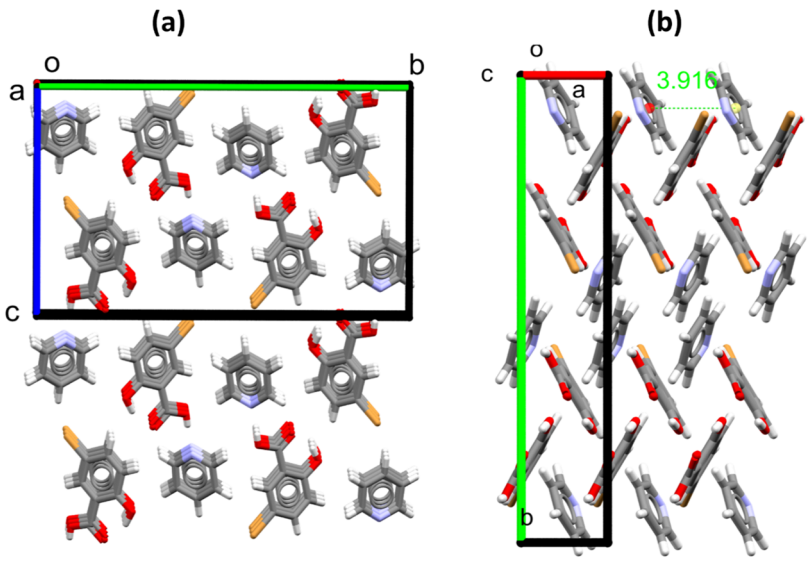

Figure 5. Crystal packing of **5** viewed along the (a) *a* axis and (b) *c* axis.

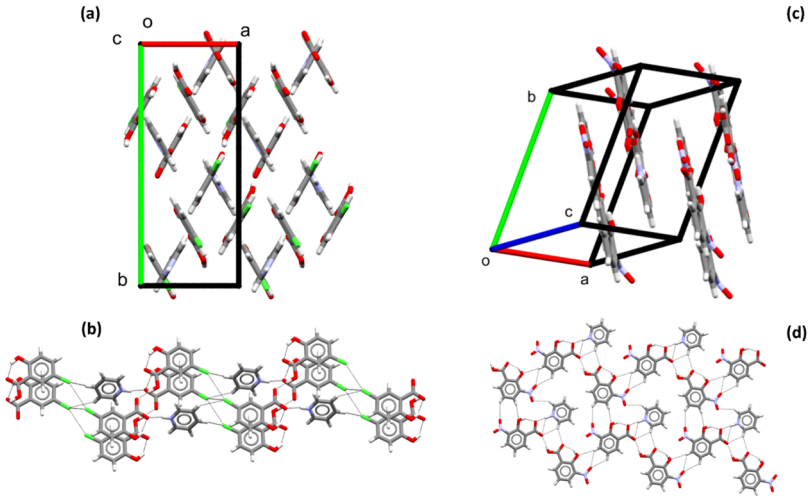

Figure 6. Ionic cocrystal packing and intermolecular interactions. (a) Crystal packing of **2** viewed along the *c* axis, (b) H bond and halogen bond patterns, (c) crystal packing of **6**, and (d) H bond in the layer of **6**.

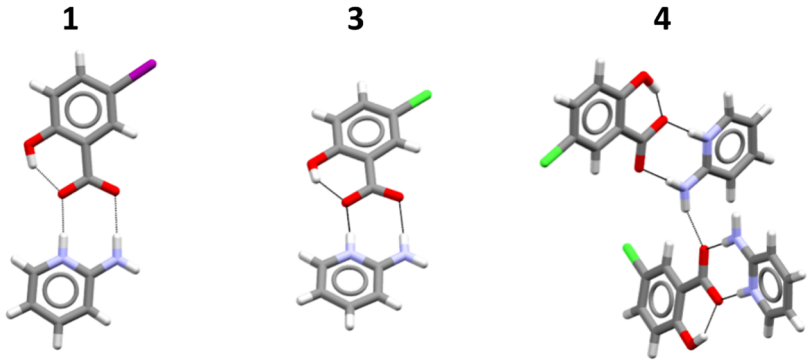

Figure 7. Supramolecular synthons in **1**, **3**, and **4**.

aminopyridine, the high basicity of 4-aminopyridine (pK_a = 9.17) led exclusively to salt formation ($\Delta pK_a > 4$). In contrast, in the systems investigated here, the choice of less basic **Py** and **2APy** (pK_a = 5.25 and 6.85, respectively), combined with subtle differences in the acidity of the salicylic acid derivatives, makes the crystallization outcomes less predictable. As a result, a variety of chemical species and, consequently, solid forms, can be obtained.

From a structural point of view, the results confirm the versatility of salicylic acid derivatives in forming different solid-state assemblies through strong charge-assisted hydrogen-bonding interactions and ionic interactions between $N-H^+$ of

https://doi.org/10.1021/acs.cgd.5c00807
Cryst. Growth Des. 2025, 25, 7618−7627

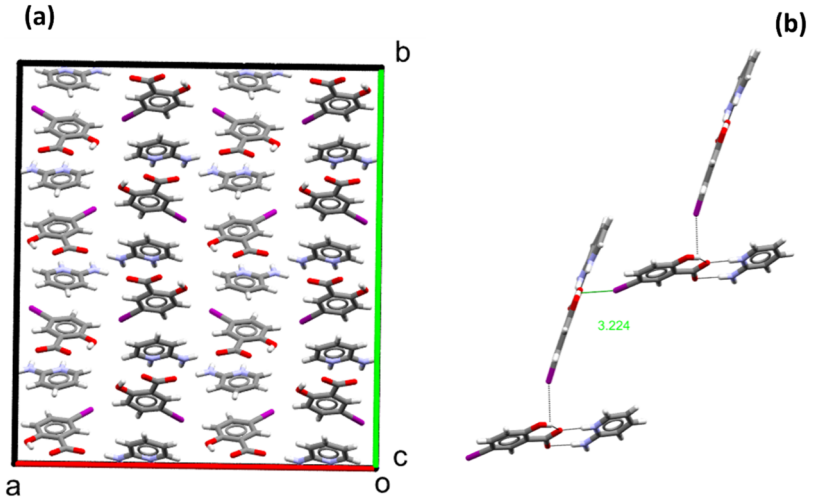

Figure 8. (a) Crystal packing of **1** viewed along the *c* axis and (b) hydrogen-bonding interaction between supramolecular dimers in **1**.

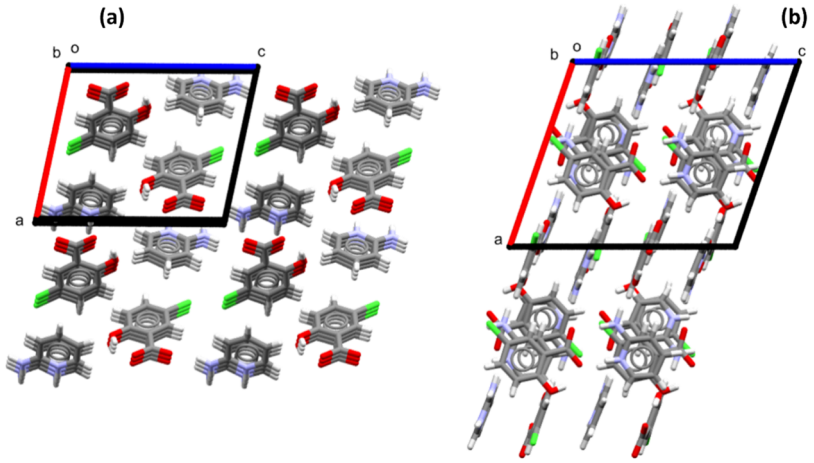

Figure 9. Crystal packing of (a) **3** and (b) **4** viewed down the *b* axis.

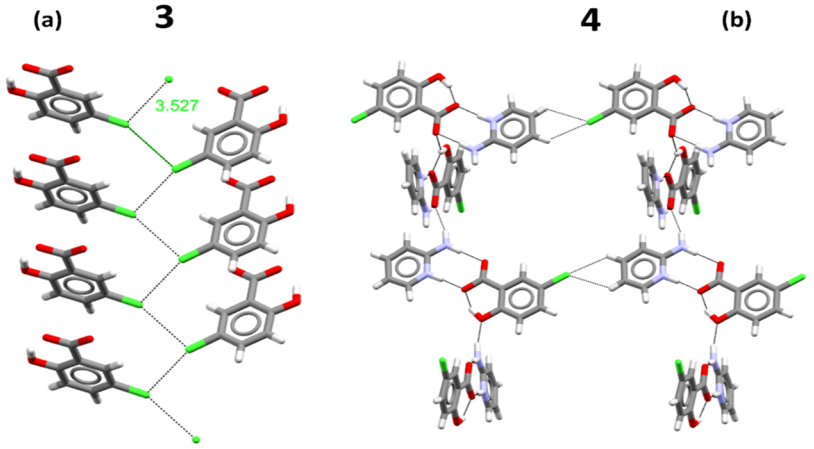

Figure 10. Supramolecular features of (a) **3** and (b) **4**.

the pyridine-based coformers and COO^- of the **SA** derivatives. The analysis of the crystal packing highlights the role of the substituents on the **SA** ring in modulating the nature and strength of the intermolecular interactions, particularly through their influence on electrostatics, hydrogen-bonding geometry, and halogen-bonding potential. The hierarchy of the supramolecular interaction in the analyzed crystal structure drives to similar self-assembly moieties, especially those involving carboxylate and $\mathbf{Py^+}/\mathbf{2APy^+}$ donors, serving as dominant structure-directing motifs.

Energy framework analysis confirms that the strongest and most consistent interaction across all structures is the $\mathbf{SA^-}$-$\mathbf{Py^+}$ interaction, which contributes significantly to the lattice stabilization. The variation in total interaction energies and

https://doi.org/10.1021/acs.cgd.5c00807
Cryst. Growth Des. 2025, 25, 7618−7627

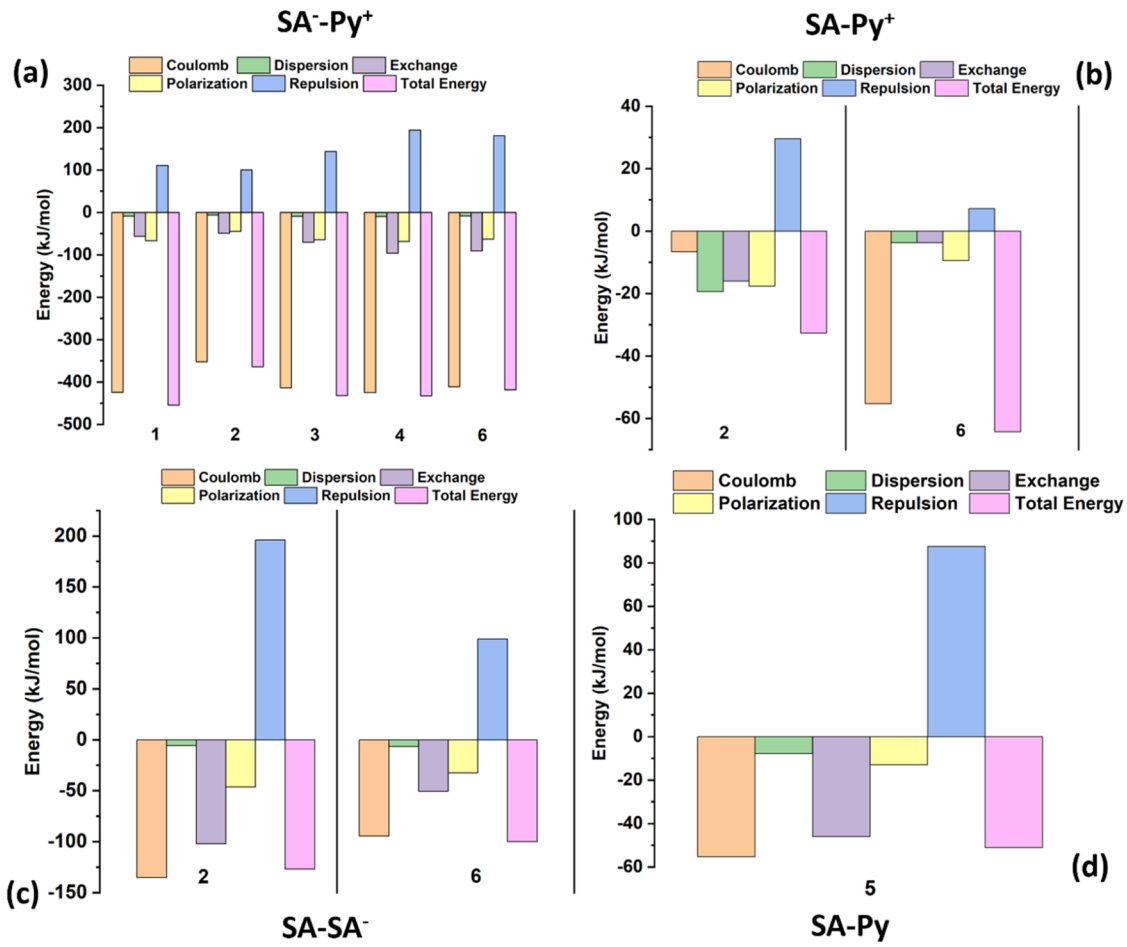

Figure 11. Contribution of Coulomb, dispersion, polarization, exchange, and repulsion interactions to the total energies of the (a) **SA⁻-Py⁺**, (b) **SA-Py⁺**, (c) **SA-SA⁻**, and (d) **SA-Py** interactions.

Table 5. Interaction Energy Contributions of the Six Novel Adducts

	Coulomb (kJ/mol)	dispersion (kJ/mol)	exchange (kJ/mol)	polarization (kJ/mol)	repulsion (kJ/mol)	tot. energy (kJ/mol)
			SA⁻-Py⁺			
1	−424.1	−8.8	−56.2	−66.5	110.8	−454.6
2	−352.1	−6.1	−49	−44.6	100.5	−363.7
3	−413.9	−9.3	−70.4	−64.2	143.7	−431.7
4	−424.5	−9.6	−96.2	−68.4	194.0	−432.5
6	−411.0	−8.1	−90.7	−63.2	180.9	−418.2
			SA-Py⁺			
2	−6.6	−19.4	−16.0	−17.6	29.6	−32.7
6	−55.3	−3.7	−3.7	−9.4	7.2	−64.3
			SA-SA⁻			
2	−135.3	−5.9	−102.2	−46.4	196.1	−126.9
6	−94.5	−6.6	−50.5	−32.6	98.9	−100.0
			SA-Py			
5	−55.3	−7.8	−46.1	−13.0	87.6	−51.1

hydrogen-bonding distances across different crystal forms demonstrates how crystal packing and molecular geometry influence the energetics of crystal formation. Overall, this investigation deepens the understanding of structure−property relationships in organic salts and ionic cocrystals, emphasizing the predictive power of crystal engineering principles based on supramolecular synthons. The results offer valuable insights for the rational design of multicomponent crystals with potential applications in pharmaceutical and nutraceutical development, where differences in the solid state influence bioavailability, stability, and manufacturability.

■ ASSOCIATED CONTENT

Supporting Information

The Supporting Information is available free of charge at https://pubs.acs.org/doi/10.1021/acs.cgd.5c00807.

pK_a table and hydrogen bond statistics plots (PDF)

https://doi.org/10.1021/acs.cgd.5c00807
Cryst. Growth Des. 2025, 25, 7618−7627

Accession Codes

Deposition Numbers 2429637 and 2429654−2429658 contain the supplementary crystallographic data for this paper. These data can be obtained free of charge via the joint Cambridge Crystallographic Data Centre (CCDC) and Fachinformationszentrum Karlsruhe Access Structures service.

■ AUTHOR INFORMATION

Corresponding Authors

Emmanuele Parisi − *Dipartimento di Scienze Applicate e Tecnologia (DISAT), Politecnico di Torino, I-10129 Torino, Italy;* orcid.org/0000-0002-9413-1372; Email: emmanuele.parisi@polito.it

Riccardo Montis − *Dipartimento di Scienze Pure e Applicate (DiSPEA), Università degli Studi di Urbino Carlo Bo, I-61029 Urbino, Italy;* orcid.org/0000-0001-5239-1849; Email: riccardo.montis@uniurb.it

Luca Catalano − *Dynamic Molecular Materials Laboratory, Dipartimento di Scienze della Vita, Università degli Studi di Modena e Reggio Emilia, I-41125 Modena, Italy;* orcid.org/0000-0002-1003-6512; Email: luca.catalano@unimore.it

Complete contact information is available at: https://pubs.acs.org/10.1021/acs.cgd.5c00807

Notes

The authors declare no competing financial interest.

■ ACKNOWLEDGMENTS

L.C. thanks the University of Modena and Reggio Emilia for financial support.

■ REFERENCES

(1) Goldschmidt, V. M. Die Gesetze Der Krystallochemie. *Naturwissenschaften* **1926**, *14* (21), 477−485.

(2) Hassel, O. Crystal chemistry. By Dr. O. Hassel. Translated by Dr. R. C. Evans, B.Sc. xi + 94. London: William Heinemann, Ltd. 1935. 6s. *J. Soc. Chem. Ind.* **1935**, *55*, No. 349.

(3) Bragg, S. W. H. The Structure of Organic Crystals. *Proc. Phys. Soc.* **1921**, *34*, 33−50.

(4) Nangia, A. Conformational Polymorphism in Organic Crystals. *Acc. Chem. Res.* **2008**, *41* (5), 595−604.

(5) Sarma, B.; Nath, N. K.; Bhogala, B. R.; Nangia, A. Synthon Competition and Cooperation in Molecular Salts of Hydroxybenzoic Acids and Aminopyridines. *Cryst. Growth Des.* **2009**, *9* (3), 1546−1557.

(6) Hursthouse, M. B.; Montis, R.; Tizzard, G. J. Intriguing Relationships and Associations in the Crystal Structures of a Family of Substituted Aspirin Molecules. *CrystEngComm* **2010**, *12* (3), 953−959.

(7) Hursthouse, M. B.; Montis, R.; Tizzard, G. J. Further Crystal Structures for the Substituted Aspirin Family of Molecules: The First Aspirin Carboxylate Catemer and a Detailed Assessment of the Subtle Influences of Weak Intermolecular Interactions. *CrystEngComm* **2011**, *13* (10), 3390−3401.

(8) Parisi, E.; Carella, A.; Borbone, F.; Chiarella, F.; Gentile, F. S.; Centore, R. Effect of Chalcogen Bonding on the Packing and Coordination Geometry in Hybrid Organic-Inorganic Cu(II) Networks. *CrystEngComm* **2022**, *24* (15), 2884−2890.

(9) Gelbrich, T.; Hursthouse, M. B. A versatile procedure for the identification, description and quantification of structural similarity in molecular crystals. *CrystEngComm* **2005**, *7*, 324−336.

(10) Gelbrich, T.; Hursthouse, M. B. Systematic investigation of the relationships between 25 crystal structures containing the carbamazepine molecule or a close analogue: a case study of the XPac method. *CrystEngComm* **2006**, *8*, 448−460.

(11) Bučar, D.-K. Engineering Molecular Crystals: Backbreaking, yet Gratifying. *Cryst. Growth Des.* **2017**, *17*, 2913−2918.

(12) Corpinot, M. K.; Bučar, D.-K. A Practical Guide to the Design of Molecular Crystals. *Cryst. Growth Des.* **2019**, *19* (2), 1426−1453.

(13) Parisi, E.; Santagata, E.; Simone, E.; Borbone, F.; Centore, R. Frustration of H-Bonding and Frustrated Packings in a Hexamorphic Crystal System with Reversible Crystal−Crystal Transitions. *J. Am. Chem. Soc.* **2024**, *146* (28), 19405−19413.

(14) Prandini, E.; Calì, E.; Maloney, A. G. P.; Parisi, E.; Simone, E. Predicting Particle Quality Attributes of Organic Crystalline Materials Using Particle Informatics. *Powder Technol.* **2024**, *443*, No. 119927.

(15) Preston, J. A.; Parisi, E.; Murray, B.; Tyler, A. I. I.; Simone, E. Elucidating the Polymorphism of Xanthone: A Crystallization and Characterization Study. *Cryst. Growth Des.* **2024**, *24* (8), 3256−3268.

(16) Beran, G. J. O. Frontiers of Molecular Crystal Structure Prediction for Pharmaceuticals and Functional Organic Materials. *Chem. Sci.* **2023**, *14*, 13290−13312.

(17) Day, G. M. Current Approaches to Predicting Molecular Organic Crystal Structures. *Crystallogr. Rev.* **2011**, *17* (1), 3−52.

(18) Parisi, E.; Borbone, F.; Carella, A.; Lettieri, S.; Capobianco, A.; Peluso, A.; Centore, R. Winning Strategy toward Acentric Crystals: Transverse Dipole Moment Molecules. *Cryst. Growth Des.* **2023**, *23* (6), 4538−4544.

(19) Montis, R.; Hursthouse, M. B. Surprisingly Complex Supramolecular Behaviour in the Crystal Structures of a Family of Mono-Substituted Salicylic Acids. *CrystEngComm* **2012**, *14* (16), 5242−5254.

(20) Bolla, G.; Sarma, B.; Nangia, A. K. Crystal Engineering of Pharmaceutical Cocrystals in the Discovery and Development of Improved Drugs. *Chem. Rev.* **2022**, *122* (13), 11514−11603.

(21) Sinha, A. S.; Maguire, A. R.; Lawrence, S. E. Cocrystallization of Nutraceuticals. *Cryst. Growth Des.* **2015**, *15* (2), 984−1009.

(22) Almarsson, r.; Zaworotko, M. J. Crystal Engineering of the Composition of Pharmaceutical Phases. Do Pharmaceutical Co-Crystals Represent a New Path to Improved Medicines? *Chem. Commun.* **2004**, *17*, 1889−1896.

(23) Chezanoglou, E.; Goula, A. M. Co-crystallization in sucrose: A promising method for encapsulation of food bioactive components. *Trends Food Sci. Technol.* **2021**, *114*, 262−274.

(24) Montisci, F.; Menicucci, F.; Carraro, C.; Prencipe, M.; Pelegatti, P.; Ienco, A.; Palagano, E.; Raio, A.; Michelozzi, M.; Mazzeo, P. P.; Bacchi, A. Effectiveness of Essential Oil Component Cocrystals Against Food Spoilage Bacteria. *Adv. Sustainable Syst.* **2024**, *8*, No. 2400002.

(25) Desiraju, G. R. Crystal Engineering: Structure, Property and Beyond. *IUCrJ.* **2017**, *4* (6), 710−711.

(26) Clarke, H. D.; K Arora, K. K.; Bass, H.; Kavuru, P.; Ong, T. T.; Pujari, T.; Wojtas, L.; Zaworotko, M. J. Structure−Stability Relationships in Cocrystal Hydrates: Does the Promiscuity of Water Make Crystalline Hydrates the Nemesis of Crystal Engineering? *Cryst. Growth Des.* **2010**, *10* (5), 2152−2167.

(27) Yu, P.; Zhen, Y.; Dong, H.; Hu, W. Crystal Engineering of Organic Optoelectronic Materials. *Chem* **2019**, *5* (11), 2814−2853.

(28) Biradha, K.; Santra, R. Crystal Engineering of Topochemical Solid State Reactions. *Chem. Soc. Rev.* **2013**, *42* (3), 950−967.

(29) Remenar, J. F.; Morissette, S. L.; Peterson, M. L.; Moulton, B.; MacPhee, J. M.; Guzmán, H. R.; Almarsson, Ö. Crystal Engineering of Novel Cocrystals of a Triazole Drug with 1,4-Dicarboxylic Acids. *J. Am. Chem. Soc.* **2003**, *125* (28), 8456−8457.

(30) Childs, S. L.; Chyall, L. J.; Dunlap, J. T.; Smolenskaya, V. N.; Stahly, B. C.; Stahly, G. P. Crystal Engineering Approach to Forming Cocrystals of Amine Hydrochlorides with Organic Acids. Molecular Complexes of Fluoxetine Hydrochloride with Benzoic, Succinic, and Fumaric Acids. *J. Am. Chem. Soc.* **2004**, *126* (41), 13335−13342.

(31) Klitou, P.; Rosbottom, I.; Simone, E. Synthonic Modeling of Quercetin and Its Hydrates: Explaining Crystallization Behavior in Terms of Molecular Conformation and Crystal Packing. *Cryst. Growth Des.* **2019**, *19* (8), 4774−4783.

(32) Klitou, P.; Pask, C. M.; Onoufriadi, L.; Rosbottom, I.; Simone, E. Solid-State Characterization and Role of Solvent Molecules on the

Crystal Structure, Packing, and Physiochemical Properties of Different Quercetin Solvates. *Cryst. Growth Des.* **2020**, *20* (10), 6573−6584.
(33) Montis, R.; Hursthouse, M. B. Crystalline Adducts of Some Substituted Salicylic Acids with 4-Aminopyridine, Including Hydrates and Solvates: Contact and Separated Ionic Complexes with Diverse Supramolecular Synthons. *CrystEngComm* **2012**, *14* (21), 7466−7478.
(34) Aakeröy, C. B.; Hussain, I.; Forbes, S.; Desper, J. Exploring the Hydrogen-Bond Preference of N−H Moieties in Co-Crystals Assembled via O−H(Acid)···N(Py) Intermolecular Interactions. *CrystEngComm* **2007**, *9* (1), 46−54.
(35) de Oliveira, Y. S.; Costa, W. S.; Borges, P. F.; de Santana, M.; Ayala, A. P. The Design of Novel Metronidazole Benzoate Structures: Exploring Stoichiometric Diversity. *Acta Crystallogr., Sect. C: Struct. Chem.* **2019**, *75* (5), 483−495.
(36) Saha, S.; Desiraju, G. R. Using Structural Modularity in Cocrystals to Engineer Properties: Elasticity. *Chem. Commun.* **2016**, *52* (49), 7676−7679.
(37) Dale, S. H.; Elsegood, M. R. J.; Hemmings, M.; Wilkinson, A. L. The Co-Crystallisation of Pyridine with Benzenepolycarboxylic Acids: The Interplay of Strong and Weak Hydrogen Bonding Motifs. *CrystEngComm* **2004**, *6* (36), 207−214.
(38) Daolio, A.; Prencipe, M.; Abodunrin, T.; Pelegatti, P.; Mazzeo, P. P.; Bacchi, A. Salt or Cocrystal Puzzle Solved by Mechanochemistry: The Role of Solvent in the Pamoic Acid Case Study. *Chem. - Eur. J.* **2025**, *31*, No. e2025000956.
(39) Shattock, T. R.; Arora, K. K.; Vishweshwar, P.; Zaworotko, M. J. Hierarchy of Supramolecular Synthons: Persistent Carboxylic Acid··· Pyridine Hydrogen Bonds in Cocrystals That Also Contain a Hydroxyl Moiety. *Cryst. Growth Des.* **2008**, *8* (12), 4533−4545.
(40) Mackenzie, C. F.; Spackman, P. R.; Jayatilaka, D.; Spackman, M. A. CrystalExplorer Model Energies and Energy Frameworks: Extension to Metal Coordination Compounds, Organic Salts, Solvates and Open-Shell Systems. *IUCrJ.* **2017**, *4* (5), 575−587.
(41) Hooft, R. *COLLECT: Data Collection and Processing User Interface*, Collect: Data collection software, Nonius BV 1998.
(42) Duisenberg, A. J. M. Indexing in Single-Crystal Diffractometry with an Obstinate List of Reflections. *J. Appl. Crystallogr.* **1992**, *25* (2), 92−96.
(43) Otwinowski, Z.; Minor, W. Processing of X-Ray Diffraction Data Collected in Oscillation Mode. In *Methods in Enzymology*; Academic Press, 1997; Vol. *276*, pp 307−326.
(44) Sheldrick, G. M. Crystal Structure Refinement with SHELXL. *Acta Crystallogr., Sect. C: Struct. Chem.* **2015**, *71* (Md), 3−8.
(45) Bruker-Nonius. *SADAB*; Bruker-Nonius: Delft, The Netherlands, 2002.
(46) Https://Github.Com/Peterspackman/Crystalexplorer/Releases.
(47) Turner, M. J.; Grabowsky, S.; Jayatilaka, D.; Spackman, M. A. Accurate and Efficient Model Energies for Exploring Intermolecular Interactions in Molecular Crystals. *J. Phys. Chem. Lett.* **2014**, *5* (24), 4249−4255.
(48) Cruz-Cabeza, A. J. Acid−base crystalline complexes and the pK_a rule. *CrystEngComm* **2012**, *14*, 6362−6365.
(49) Cruz-Cabeza, A. J.; Lusi, M.; Wheatcroft, H. P.; Bond, A. The role of solvation in proton transfer reactions: implications for predicting salt/co-crystal formation using the ΔpK_a rule. *Faraday Discuss.* **2022**, *235*, 446−466.
(50) Bhogala, B. R.; Basavoju, S.; Nangia, A. Tape and layer structures in cocrystals of some di- and tricarboxylic acids with 4,4′-bipyridines and isonicotinamide. From binary to ternary cocrystals. *CrystEngComm* **2005**, *7*, 551−562.
(51) Mukherjee, A.; Desiraju, G. R. Combinatorial Exploration of the Structural Landscape of Acid−Pyridine Cocrystals. *Cryst. Growth Des.* **2014**, *14* (3), 1375−1385.

https://doi.org/10.1021/acs.cgd.5c00807
Cryst. Growth Des. 2025, 25, 7618−7627